Role of the Met−Tyr−Trp Cross-Link in Mycobacterium tuberculosis Catalase-Peroxidase (KatG) As Revealed by KatG(M255I) †

ARTICLE *in* BIOCHEMISTRY · DECEMBER 2005

Impact Factor: 3.02 · DOI: 10.1021/bi051463q · Source: PubMed

3 AUTHORS, INCLUDING:

Paul R. Ortiz de Montellano
University of California, San Francisco
479 PUBLICATIONS **17,539** CITATIONS

Role of the Met−Tyr−Trp Cross-Link in *Mycobacterium tuberculosis* Catalase-Peroxidase (KatG) As Revealed by KatG(M255I)†

Reza A. Ghiladi, Katalin F. Medzihradszky, and Paul R. Ortiz de Montellano*

Department of Pharmaceutical Chemistry, University of California, San Francisco, California 94143-2280

Received July 25, 2005; Revised Manuscript Received September 16, 2005

ABSTRACT: Catalase-peroxidases (KatGs) are bifunctional enzymes possessing both catalase and peroxidase activities. Four crystal structures of different KatGs revealed the presence of a novel Met−Tyr−Trp cross-link which has been suggested to impart catalatic activity to the KatGs. To decipher the individual roles of the two cross-links in the Met−Tyr−Trp adduct, we have focused on recombinant *Mycobacterium tuberculosis* KatG(M255I). UV−visible spectroscopic and mass spectrometric studies of the peptide fragments resulting from tryptic digestion of KatG(M255I) confirmed the presence of the single Tyr−Trp cross-link, as well as a $2e^-$ oxidized form which is postulated to be an intermediate generated during Met−Tyr−Trp cross-link formation. KatG(M255I) lacking the Tyr−Trp cross-link was also prepared, and incubation with peroxyacetic acid, but not 2-methyl-1-phenyl-2-propyl hydroperoxide, resulted in complete formation of the Tyr−Trp cross-link. A mechanism for Tyr−Trp autocatalytic formation by KatG compound I is proposed from these studies. Optical stopped-flow studies with KatG(M255I) were performed, allowing characterization of compounds I, II, and III. Interestingly, two compound II intermediates were identified: (KatG•)(Por)Fe^{III}-OH, where KatG• represents a protein-based radical, and oxoferryl (KatG)(Por)Fe^{IV}═O. Insight into the contributions of the individual Tyr−Trp and Met−Tyr cross-links to catalase activity is presented, as is the overall contribution of the Met−Tyr−Trp cross-link to the structure−function−spectroscopy relationship and catalase-peroxidase mechanism in KatG.

Catalase-peroxidases (KatGs)[1] are bifunctional hemoproteins belonging to class I of the peroxidase superfamily (plants, fungi, and bacteria) and exhibit both catalatic ($H_2O_2 \rightarrow H_2O + {}^1/_2O_2$) and peroxidatic ($2AH + H_2O_2 \rightarrow 2A^\bullet + 2H_2O$) activities (*1*). KatGs are anomalies: they have a high degree of sequence homology with eukaryotic peroxidases, including fungal cytochrome *c* peroxidase and plant ascorbate peroxidase (*2*), and as such possess substantial peroxidase activity, yet they also exhibit catalatic activity equivalent to that of the monofunctional catalases despite having little sequence homology with the latter (*3*). Additional enzymatic functions for KatGs have been described, including Mn^{2+}-dependent peroxidase (*4*, *5*), cytochrome P450-like oxygenase (*6*), and peroxynitritase activities (*7*).

The crystal structures of KatG from *Haloarcula marismortui* (*8*), *Burkholderia pseudomonas* (*9*), *Synechococcus* PCC 7942 (*10*), and *Mycobacterium tuberculosis* (*11*) each show the presence of two covalent bonds between three amino acid side chains, Trp107, Tyr229, and Met255 (*Mtb* numbering), located on the distal side of the heme active site (Figure 1). The consistent observation of this Met−Tyr−Trp cross-link suggests that it is a characteristic common to all KatGs. As such, KatG is one of a growing number of metalloenzymes that have aromatic amino acids covalently modified in their active sites. Cytochrome *c* oxidase (His240−Tyr244; $heme_{a3}-Cu_B$) (*12*−*14*), catalase HPII (His392−Tyr415; heme) (*15*), galactose oxidase (Tyr272−Cys228; copper) (*16*, *17*), catalase-1 (Cys356−Tyr379; heme) (*18*), and amine oxidase (2,4,5-trihydroxyphenylalanine quinone; copper) (*19*) are but a few examples. Side chain covalent bond formation in these systems is believed to occur through metal-mediated autocatalytic processes, with the resulting modified amino acids possessing altered redox and pK_a properties that affect enzyme chemistry (*20*−*23*).

We have previously (*24*) demonstrated that the Met−Tyr−Trp cross-link forms in an autocatalytic process that is solely dependent upon compound I [(Por•)Fe^{IV}═O, oxoferryl porphyrin π-cation radical] as the oxidizing species, and we proposed a mechanism for its formation on the basis of these results. The presence (WT KatG) or absence [KatG(Y229F)] of the Met−Tyr−Trp cross-link also had a marked effect on the UV−visible spectrum of compound II, which we interpreted as two distinct electronic states, either as (KatG•)(Por)Fe^{III}-OH for WT KatG or as (KatG)(Por)Fe^{IV}═O for KatG(Y229F). Additionally, as we and others (*25*−*28*) have noted, the absence of the cross-link completely abolishes

† This work was supported by NIH Grant AI58524 (R.A.G., F32-Postdoctoral Fellowship), NCRR RR001614 and RR012961 (K.F.M., to the UCSF Mass Spectrometry Facility, director A. L. Burlingame), and GM56531 and GM32488 (P.R.O.d.M.).

* To whom correspondence should be addressed: Department of Pharmaceutical Chemistry, University of California, San Francisco, 600 16th St., San Francisco, CA 94143-2280. Telephone: (415) 476-2903. Fax: (415) 502-4728. E-mail: ortiz@cgl.ucsf.edu.

[1] Abbreviations: KatG, catalase-peroxidase; *Mtb*, *Mycobacterium tuberculosis*; HPII, hydroperoxidase II; Por, porphyrin; WT, wild-type; MPPH, 2-methyl-1-phenyl-2-propyl hydroperoxide; ^{R}KatG(M255I), heme-reconstituted KatG(M255I); PAA, peroxyacetic acid; CLPF, cross-linked peptide fragment; R_z, Reinheitzahl; HS, high-spin; ABTS, 2,2′-azinobis(3-ethylbenzothiazoline-6-sulfonate); CID, collision-induced dissociation; ^{QL}Tyr−Trp, quinone-like Tyr−Trp (a two-electron-oxidized form of the Tyr−Trp cross-link); EPR, electron paramagnetic resonance.

10.1021/bi051463q CCC: $30.25
Published on Web 10/25/2005

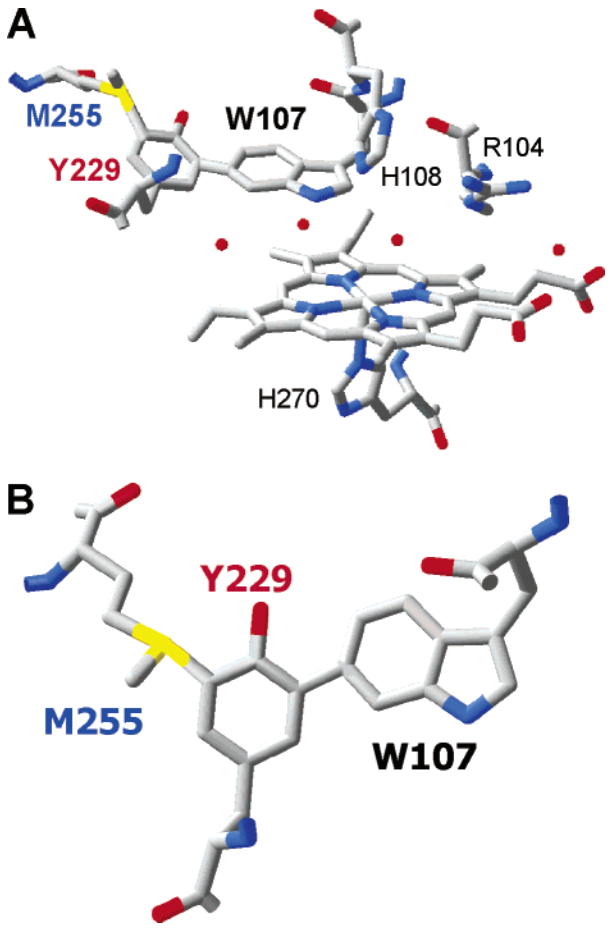

FIGURE 1: Active site of *Mtb* KatG (A) depicting the Met−Tyr−Trp cross-link (B) and its proximity to the heme cofactor. Coordinates were obtained from the Protein Data Bank (entry 1SJ2) and displayed using the Swiss PDB Viewer.

catalase (but not peroxidase) activity and, as it is not found in the monofunctional peroxidases, implies that this structural element imparts catalatic activity to the KatGs (*11*). Thus, a structure−function−spectroscopy relationship exists in the KatGs that is not observed in other peroxidases. Namely, the presence of the cross-link correlates with both catalase activity and compound II being (KatG$^{\bullet}$)(Por)Fe^{III}-OH ("catalase-peroxidase-like"), whereas the absence of the cross-link leads to only peroxidase activity, as well as observation of an oxoferryl compound II [(KatG)(Por)Fe^{IV}=O] intermediate, similar to that observed in the monofunctional peroxidases.

Despite the progress made in understanding this structure−function−spectroscopy relationship, many questions still need to be addressed. How does the cross-link impart catalase activity to what is essentially a peroxidase? What role does the sulfonium ion play in the Met−Tyr−Trp cross-link? In its absence, what will be the effect on the spectral features of compound II? Can we deconvolute the contributions of the Tyr−Trp cross-link to autocatalytic formation, enzyme catalysis, and spectroscopy from those of the Met−Tyr−Trp cross-link? If so, can we detect any Tyr−Trp species that may act as an intermediate in Met−Tyr−Trp cross-link formation? To address these and other questions, we describe here our biochemical and spectroscopic investigations of KatG(M255I), whose Met → Ile mutation leads only to Tyr−Trp cross-link formation. We have employed stopped-flow UV−visible spectroscopy to characterize the compound I, II, and III intermediates of KatG(M255I), and have shown that this mutant leads to observation of both oxoferryl and (KatG$^{\bullet}$)(Por)Fe^{III}-OH compound II species, affording us a better understanding of the relationship between this intermediate and catalase activity. We have been able to express KatG(M255I) lacking the Tyr−Trp cross-link, and followed its formation under conditions known to generate either compound I or II, thereby allowing us to investigate the individual steps involved in the autocatalytic formation of the Met−Tyr−Trp cross-link. Thus, through comparison with WT KatG (Met−Tyr−Trp cross-link present) and KatG(Y229F) (cross-link absent), it is possible to investigate the role of just the Tyr−Trp cross-link in both enzymatic activity and spectroscopic properties of reactive intermediates, from which we can deduce the role of the Met−Tyr bond in the fully formed cross-link. The relevance of these results is discussed with respect to the catalase-peroxidase mechanism.

EXPERIMENTAL PROCEDURES

Materials. Buffer salts and acetonitrile (HPLC grade) were purchased from Fisher Scientific. All other reagents and biochemicals, unless otherwise specified, were of the highest grade available from Sigma-Aldrich. 2-Methyl-1-phenyl-2-propyl hydroperoxide (MPPH) was synthesized according to published procedures (*29*, *30*).

Plasmid Preparation, Protein Expression, and Purification. The plasmid pKatG(M255I) was prepared using mutagenic primers [5′-ATTCGCGAGACGTTTCGGCGC**ATC**GCCATGAACGACGTCGAA-3′ (sense) and 3′-GCGCCGAAACGTCTCGCGAATGTCGAC-5′ (antisense)] by PCR amplification of pMRLB11 [Colorado State University, Fort Collins, CO; National Institute of Allergy and Infectious Diseases (NIAID) Contract N01 AI-75320] under conditions identical to those reported elsewhere (*31*). Protein expression and purification were performed as previously described for WT KatG without modification (*31*, *32*).

Spectroscopic Studies. Optical spectra were recorded on a Hewlett-Packard 8452A diode array spectrophotometer equipped with a thermostated cell holder at 25 °C. Protoheme content was measured by the pyridine hemochrome assay using a $\Delta\epsilon_{557}$ of 20.7 mM^{-1} cm^{-1} (reduced − oxidized) for iron protoporphyrin IX (*33*, *34*).

Catalase and Peroxidase Activity Measurements. Measurements were carried out using a SpectraMax Plus384 96-well UV−visible plate reader as previously described (*24*, *31*). The concentrations of KatG(M255I) employed were 20 μM and 500 nM for the catalase and peroxidase activity measurements, respectively.

Tryptic Digest, HPLC Separation, and Mass Spectrometric Identification of the Tyr−Trp Adduct in KatG(M255I). In a protocol similar to that described previously for WT KatG (*24*), 250 μL of a 50 μM solution of KatG(M255I) (~1 mg of protein) in 100 mM KP$_i$ (pH 7.5) was incubated with 5 μg (200:1 protein:protease ratio) of sequencing grade modified trypsin (Promega) for 3 h at 37 °C. Following proteolytic digestion, the peptide fragments were separated using HPLC [ProSphere (Alltech) C$_{18}$, 5 μm, 100 Å; buffer A composed of H$_2$O and 0.1% trifluoroacetic acid (TFA); buffer B composed of MeCN and 0.1% TFA; linear gradient from 0 to 60% B over 4 h at 0.5 mL/min; UV−visible spectroscopic monitoring (diode array), 200−600 nm]. Fractions (~0.5−1 mL) were collected and concentrated (SpeedVac). LC−MS

analyses of the appropriate manually collected tryptic fractions were performed using a nanoHPLC system, consisting of an Eksigent nanopump and a Spark autosampler (column, C-18, 75 μm × 150 mm; solvent A composed of 0.1% formic acid in H_2O; solvent B composed of 0.1% formic acid in acetonitrile; flow rate of ~300 nL/min; linear gradient from 5 to 50% B over 30 min), and a QSTAR Pulsar (Applied Biosystems) quadrupole-orthogonal-acceleration-time-of-flight hybrid tandem mass spectrometer as a detector. Fractions were infused for CID analysis, and CID data were acquired in MCA mode with manual adjustment of the collision energy.

Overexpression of Apo-KatG(M255I) and Heme Reconstitution. Apo-KatG(M255I) deficient in heme was overexpressed, purified, and reconstituted with heme [resulting in ^{R}KatG(M255I)] as described for WT KatG without modification (*24*).

Autocatalytic Formation of the Tyr−Trp Cross-Link. A 250 μL sample of a 50 μM solution of ^{R}KatG(M255I) in 100 mM KP_i (pH 7.5) and 5 μM EDTA was incubated with peroxyacetic acid (PAA; 0, 0.5, 1.0, 1.25, 1.5, 1.75, 2.0, 2.25, 2.5, 2.75, 3.0, 4, 5, 7.5, and 10 equiv) or MPPH (4, 8, or 25 equiv) for 1 h at 25 °C. The samples were then digested with trypsin and analyzed by HPLC as described above, with the exception that a linear gradient from 30 to 38% buffer B over 25 min was employed to elute the peptide fragments containing the Tyr−Trp cross-link (CLPFs). Peptide formation was determined via peak integration (A_{220} chromatogram; area under the curve from 43 to 48 min), with 3.5 equiv (maximum value of CLPFs determined by integration) normalized to 100%. The experiment was repeated in triplicate, and the data are reported as the average ± the standard deviation.

Stopped-Flow UV−Visible Spectrophotometry. Experiments were performed on a Hi-Tech SF-61 DX2 double mixing stopped-flow system employing a diode array spectrophotometer, and were carried out at 25 °C in 100 mM KP_i (pH 7.5) containing 5 μM EDTA. The initial (premixing) concentrations were as follows: 20 μM KatG, 20, 50, or 200 μM MPPH, 20, 50, or 200 μM PAA, and 0.02, 0.2, 2, and 20 mM H_2O_2. Data were collected (300 scans) over 0.6, 6, 60, and 600 s using the KinetAsyst software package (Hi-Tech), and analyzed using the Specfit Global Analysis System software package (Spectrum Software Associates) as pseudo-first-order reactions and fit from one to three exponential curves where applicable.

RESULTS

UV−Visible Spectroscopic Analysis of KatG(M255I). The electronic absorption spectrum of KatG(M255I) is shown in Figure 2, and is contrasted with those observed for WT KatG (Met−Tyr−Trp cross-link present) and KatG(Y229F) (Met−Tyr−Trp cross-link absent). Relevant spectral features and analysis are presented in Table S1 of the Supporting Information. The optical purity ratio (Reinheitzahl or R_z, defined as A_{Soret}/A_{280}) for KatG(M255I) was found to be 0.56. The pyridine hemochrome assay of KatG(M255I) yielded 0.97 ± 0.04 heme/monomer, indicating stoichiometric heme incorporation, suggesting that the slightly lower R_z value when compared to that of WT KatG (0.63) or KatG(Y229F) (0.59) is most likely due to a smaller heme extinction and not the presence of the apoenzyme.

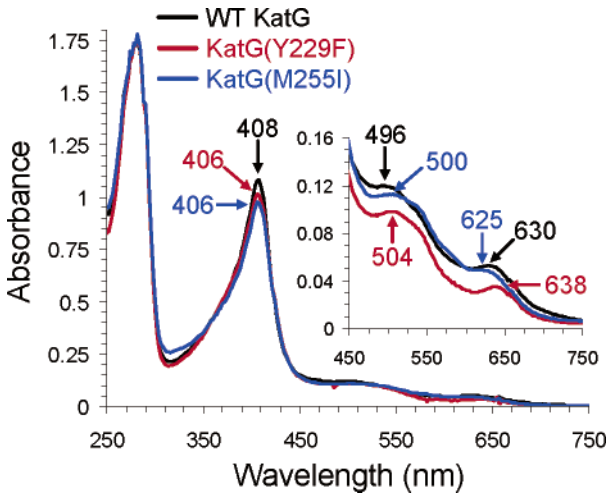

FIGURE 2: UV−visible spectra of KatG(M255I) (blue), WT KatG (black), and KatG(Y229F) (red). Conditions: 10 μM enzyme in 100 mM potassium phosphate at pH 7.5 and 25 °C.

Table 1: Kinetic Parameters for Catalase and Peroxidase Activities of KatG(M255I) and ^{R}KatG(M255I)

	KatG(M255I)	^{R}KatG(M255I)
	Catalase	
k_{cat} (s^{-1})	1.1 ± 0.1	1.0 ± 0.1
K_m (mM)	40.2 ± 6.1	37.3 ± 8.8
k_{cat}/K_m (M^{-1} s^{-1})	27.0 ± 4.1	26.8 ± 6.3
	Peroxidase	
k_{cat} (s^{-1})	0.164 ± 0.002	0.157 ± 0.001
K_m (mM)	3.40 ± 0.08	3.30 ± 0.05
k_{cat}/K_m (M^{-1} s^{-1})	48.1 ± 1.2	46.1 ± 0.7

In lieu of electron paramagnetic or resonance Raman spectroscopic studies, analysis of the UV−visible spectrum of KatG(M255I) by the methodology employed by Magliozzo and co-workers (*35*) provides insight into the electronic nature of the heme prosthetic group. KatG(M255I) (A_{614}/A_{645} = 1.19) (Table S1) has a significantly greater relative population of six-coordinate HS heme present than either WT KatG (1.05) or KatG(Y229F) (0.85), with all three lacking a detectable (by optical spectroscopy) low-spin heme component. The narrow range of the A_{Soret}/A_{380} ratio (1.68−1.79) precludes any relative population assignments.

Catalase and Peroxidase Activities of KatG(M255I). Kinetic parameters (k_{cat}, K_m, and catalytic efficiency, k_{cat}/K_m) for the catalase and peroxidase activities of KatG(M255I) are presented in Table 1. As conventional catalases do not follow typical Michaelis−Menten kinetics, kinetic constants reported here for catalase activity are "apparent" values (*36*, *37*). KatG(M255I) exhibited saturable catalase activity under the conditions employed for this kinetic study. The k_{cat} (1.1 ± 0.1 s^{-1}) and K_m (40.2 ± 6.1 mM) values are similar to those reported for KatG(Y229F) (Met−Tyr−Trp cross-link absent; 0.1 s^{-1} and 39.8 mM, respectively), but are significantly different from those observed for WT KatG (Met−Tyr−Trp cross-link present; 6000 s^{-1} and 2.5 mM, respectively). The result that catalase activity is severely disrupted for KatG(M255I) versus WT KatG (k_{cat}/K_m ~10^5 lower) is consistent with literature observations (*26*, *28*, *38*) which show that an intact Met−Tyr−Trp cross-link is essential for catalatic activity.

KatG(M255I) exhibited saturable peroxidase activity for the one-electron oxidation of ABTS to the corresponding

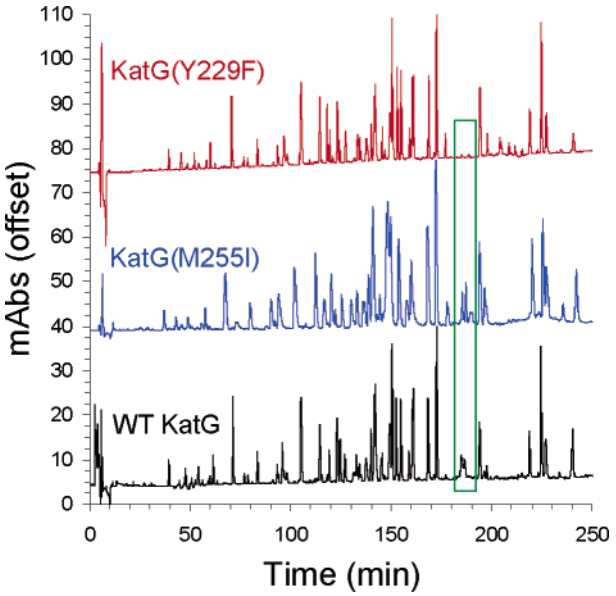

FIGURE 3: HPLC chromatogram (A_{220} detection) of the tryptic digest of KatG(M255I) (middle). A detailed enlargement of the area between 100 and 200 min is provided in Figure 5A. For comparison, the chromatograms of WT KatG (bottom) and KatG(Y229F) (top) are also shown. The region around 185 min, corresponding to the CLPF, is highlighted.

radical cation, $ABTS^{\bullet+}$, in the presence of *tert*-butyl hydroperoxide. An increase in k_{cat} (0.164 ± 0.002 s^{-1}) and a decrease in K_m (3.4 ± 0.1 mM) were noted for KatG(M255I) when compared to those of the wild-type enzyme (0.062 s^{-1} and 8.4 mM, respectively), but not to the extent of those observed for KatG(Y229F) (0.843 s^{-1} and 2.7 mM, respectively). The increase in peroxidase activity for *Mtb* KatG(Y229F) has been noted previously by Magliozzo and coworkers (*38*), who suggested that upon loss of the covalent adduct the increase in peroxidase activity (with a concomitant loss of catalase function) is due to enhanced formation and/or an increased level of stabilization of the compound II intermediate, which plays a role in the peroxidase, but not catalase, cycle.

Tryptic Digestion of KatG(M255I). The HPLC chromatogram (A_{220} monitoring) of the tryptic digest of KatG(M255I) is shown in Figure 3 (blue), along with those previously reported (*24*) for WT KatG (black) and KatG(Y229F) (red). In general, the number of peptide fragments (as well as their retention times) correlated well among all three enzymes. However, in the region which we have previously assigned as containing the WT KatG Met−Tyr−Trp CLPF (cross-linked peptide fragment; Figure 3, boxed area) (*24*), KatG(M255I) also exhibits four peptides (one major and three minor) in a tight cluster which are absent from KatG(Y229F). The similarity with WT KatG and the difference with KatG(Y229F) were highly suggestive of the presence of Tyr−Trp cross-linked peptide fragments in KatG(M255I) (Figure 4B, henceforth called the Tyr−Trp CLPF), predicted from trypsin cleavage sites to incorporate ^{105}MA**W**HAAGTYR^{114} and ^{215}DLENPLAAVQMGLI**Y**VNPEGPNGNPDPMAAAVDIR^{249}. The ^{255}**M**AMNDVETAALIVGGHTFGK^{274} fragment of the Met−Tyr−Trp CLPF found in WT KatG (Figure 4A) was precluded from partaking in any cross-link in KatG(M255I) by the Met → Ile mutation.

The HPLC chromatograms of the tryptic digest of KatG(M255I), monitored at λ values of 220 (peptide backbone), 280 (tyrosine/tryptophan), and 330 nm (cross-linked peptides), are shown in Figure 5A. The Tyr−Trp CLPFs of KatG(M255I) exhibited two distinct UV−visible spectra, with unusual absorptions extending as far as 330 nm (Figure 5A, top). The major Tyr−Trp CLPF (Figure 5B, blue) had spectral features (λ_{max}) at 296 and 252 (sh) nm, similar to those observed for the Met−Tyr−Trp CLPF from WT KatG (Figure 5B, red) (*24*), but markedly different from the absorption spectrum of a "typical" peptide observed in this tryptic digest (Figure 5B, black; specifically shown is the peptide eluting at 195 min). The three minor Tyr−Trp CLPFs exhibited a UV−visible spectrum (λ_{max} = 252, 308, and 320 nm; Figure 5B, green) markedly different from that observed for either the major CLPF or the Met−Tyr−Trp CLPF. As we have discussed in detail for the Met−Tyr−Trp cross-link (*24*), the presence of these large bathochromic shifts in the UV−visible spectra of the CLPFs is suggestive of the presence of peptide cross-links. Structural differences between the two types of Tyr−Trp CLPF in KatG(M255I) were inferred from mass spectrometric studies (vide infra).

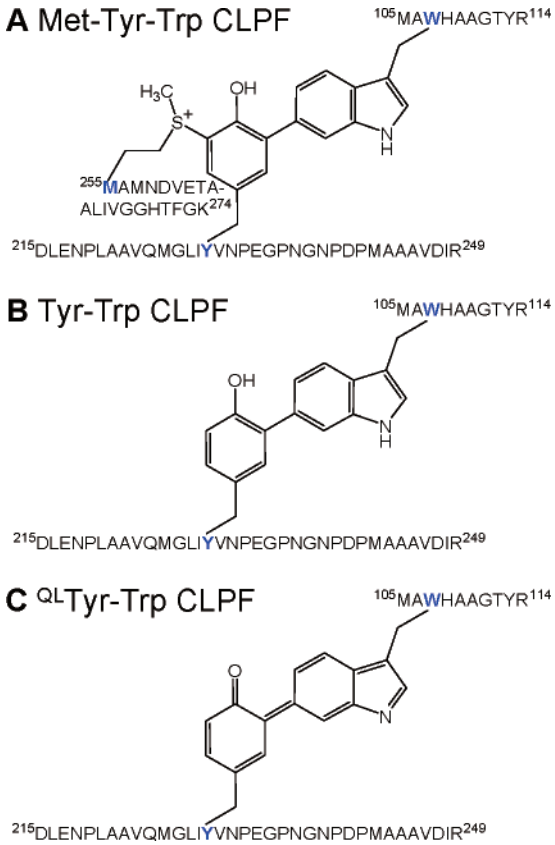

FIGURE 4: Schematic representation of the CLPFs in KatG(M255I) and WT KatG.

Mass Spectrometry. The four putative Tyr−Trp CLPFs isolated by HPLC and identified by their characteristic electronic absorptions at ~300 nm were subjected to LC−MS/MS analysis in an information-dependent manner. The calculated MH^+ value of the Tyr−Trp CLPF (Figure 4B) is 4822.31 Da. The major CLPF was represented by ions at *m*/*z* 1206.35 (4+) and 965.26 (5+) (Figure 6A, top) and yielded a monoisotopic MH^+ value (4822.4 Da), which is in good agreement with the calculated value. To prove the identity of this molecule, a CID experiment was performed using the quadruply charged ion as the precursor. The results (Figures 6B, top) provided all the necessary proof needed.

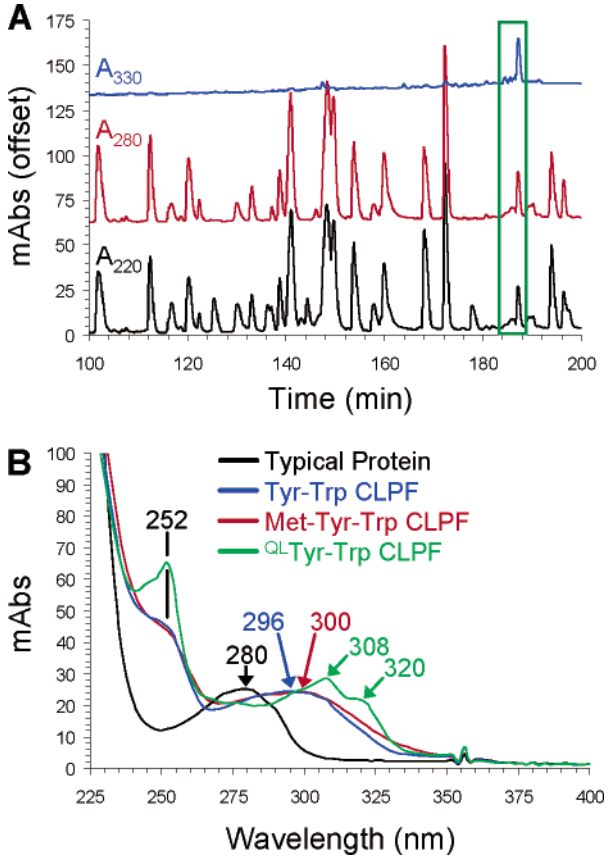

FIGURE 5: (A) HPLC chromatogram (100−200 min region) of the tryptic digest of KatG(M255I) monitored at 330 (top), 280 (middle), and 220 nm (bottom). The CLPFs at ∼185 min are highlighted. (B) UV−visible spectra of the Tyr−Trp CLPF (blue) and ^{QL}Tyr−Trp (green) are compared to that of either a peptide lacking a cross-link (black) or the Met−Tyr−Trp cross-link (red) of WT KatG.

Two of the minor isolated CLPFs were found to contain molecular ions at *m*/*z* 964.86 (5+) and 1205.83 (4+) (Figure 6A, bottom), corresponding to a MH^+ value of 4820.32 Da, or a mass 2 Da lower than that calculated for the Tyr−Trp adduct. CID experiments using the quadruply charged ion as the precursor (Figure 6B, bottom) reveal that the 2 Da lower mass is centered on the Tyr−Trp cross-link, as residues prior to Y229 [105−114 and 215−228] were found at their non-oxidized mass, while each residue identified after the Tyr−Trp cross-link was found 2 Da lower. We propose that the $2e^-$ oxidation of the Tyr−Trp CLPF would most likely result in formation of a quinone-like intermediate, best described as a ^{QL}Tyr−Trp CLPF (Figure 4C). Oxidation of the Tyr−Trp CLPF due to enzymatic turnover of the recombinant protein during overexpression would result in only the native trans conformation being observed, whereas oxidation occurring post-proteolytic digestion would yield both cis and trans conformations due to free rotation about the Cη2(Trp107)−Cϵ1(Tyr229) bond. Given that two separable peaks (∼3:1 relative area) are observed in the HPLC chromatogram, we suggest that both native trans and scrambled cis conformations of the ^{QL}Tyr−Trp CLPF are observed, with the more abundant of the two peaks probably arising from predigestion Tyr−Trp oxidation, and the less abundant one (cis) being derived from solely the postdigestion oxidation.

The final minor isolated CLPF exhibited relatively abundant ions at *m*/*z* 1051.51 (4+) and 841.20 (5+), corresponding to an MH^+ value of 4203.03 Da. We attribute this mass to a nonspecific cleavage occurring at position H108 (i.e., loss of residues 108−114) of the ^{QL}Tyr−Trp CLPF, whose calculated MH^+ value (4203.15 Da) is in good agreement with the experimentally determined mass.

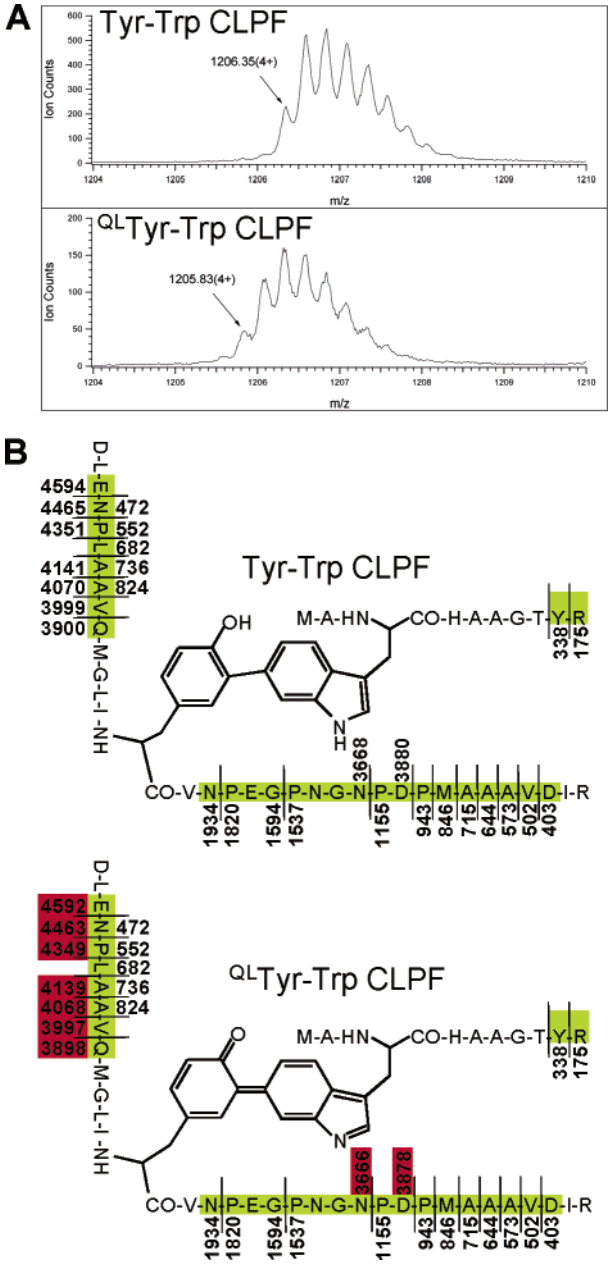

FIGURE 6: (A) Tyr−Trp CLPF [top, *m*/*z* 1206.35 (4+)] and ^{QL}Tyr−Trp CLPF [bottom, *m*/*z* 1205.83 (4+)] precursor ions for the CID (MS/MS) experiments. (B) Fragment assignments from the CID experiment for the Tyr−Trp CLPF (top) and ^{QL}Tyr−Trp CLPF (bottom). B-Type (N-terminal) ions are depicted above the corresponding amino acid residue, and y-type ions (C-terminal) are depicted below. Ions depicted in red denote the 2 Da shift to a lower mass upon oxidation of the Tyr−Trp CLPF to the ^{QL}Tyr−Trp CLPF.

Autocatalytic Formation of the Tyr−Trp Cross-Link in ^{R}KatG(M255I). The presence of the Tyr−Trp CLPFs in recombinant KatG(M255I) is most likely due to their autocatalytic formation during overexpression in *Escherichia coli* because of the presence of hydrogen peroxide or alkylhydroperoxides in the in vivo system, although the intervention of a cellular assembly system cannot be

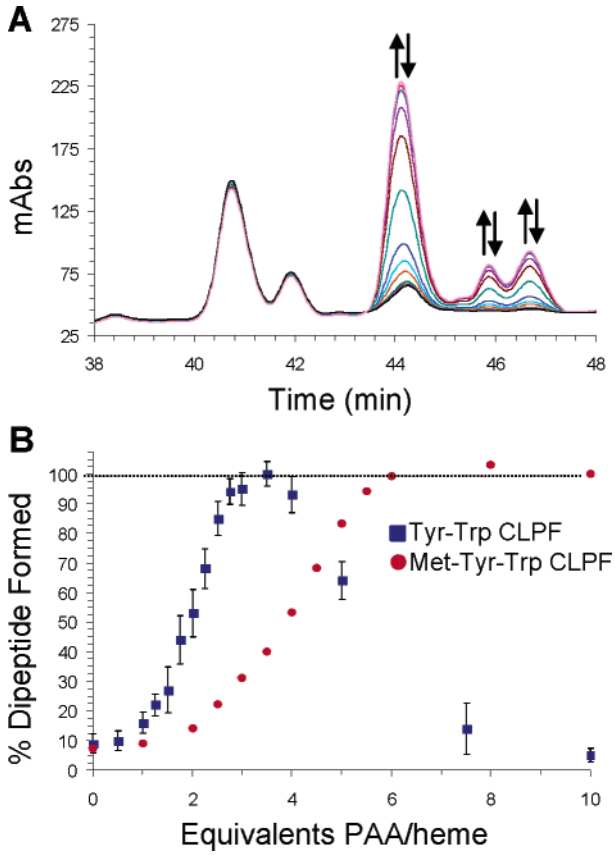

FIGURE 7: (A) HPLC chromatograms (CLPF region) of the tryptic digests of ^{R}KatG(M255I) after incubation with 0−10 equiv of PAA prior to proteolytic digestion. (B) CLPF formation as a function of PAA concentration. Maximal CLPF formation occurred at 3.5 equiv of PAA, with the remaining data normalized to this value.

excluded. Thus, to study the formation of the Tyr−Trp cross-link under controlled conditions in vitro, it was necessary to first isolate KatG(M255I) which had not undergone in vivo catalysis. The strategy employed was identical to that used for studying the autocatalytic formation of the Met−Tyr−Trp cross-link in WT KatG (*24*), namely, to overexpress and isolate heme-deficient (apo) KatG incapable of undergoing any autocatalytic processes that could generate the Tyr−Trp cross-link. Apo-KatG(M255I) grown under low-iron conditions exhibited an R_z value of 0.07 (Figure S1), indicating only 8% holoenzyme present (when compared to an R_z of 0.56 for normal growth conditions). Tryptic digestion and HPLC analysis of this heme-deficient KatG revealed only 6.1 ± 1.8% of the Tyr−Trp CLPFs formed during protein expression. Reconstitution of apo-KatG(M255I) with heme was accomplished using denaturing conditions to expose the heme-binding pocket, followed by refolding of the protein in the presence of hemin. The resulting reconstituted KatG(M255I) [henceforth called ^{R}KatG(M255I)] exhibited an R_z value (0.55) (Figure S1) and k_{cat} and K_m values for catalase and peroxidase activities consistent with those found for KatG(M255I) (Table 1).

Incubation of ^{R}KatG(M255I) with peroxyacetic acid (Figure 7A), a two-electron oxidant that leads to compound I formation in WT KatG (*39*), led to an increase in the amount of Tyr−Trp CLPFs observed after tryptic digestion and HPLC analysis (Figure 7B), with a maximum achieved after the addition of 3.5 equiv. By contrast, in the absence of PAA, only 9.0 ± 3.2% (relative to this maximum) of the CLPFs was detected, an amount nearly identical to that found for apo-KatG (6.1 ± 1.8%), indicating that heme reconstitution alone does not contribute to CLPF formation. With more than 4 equiv, however, CLPF yields diminished, with only ~5% remaining after treatment with 10 total equivalents PAA. This contrasts with the previously reported behavior observed for the Met−Tyr−Trp adduct, where the maximum level of CLPF formation was observed after the addition of 6 equiv of PAA, and remained at that level even after 25 equiv.

To determine if compound II is involved in Tyr−Trp cross-link formation, ^{R}KatG(M255I) was incubated with 4, 8, and 25 equiv of 2-methyl-1-phenyl-2-propyl hydroperoxide (MPPH), a reagent which undergoes homolytic O−O bond cleavage (*40*), preferentially yielding compound II rather than compound I (vide infra, stopped-flow UV−visible discussion). At 4 and 8 equiv of MPPH added per heme, the amount of CLPF determined was within error (8.4 ± 2.5 and 8.1 ± 2.8%, respectively) of the amount determined prior to MPPH addition (9.0 ± 3.2%). At 25 equiv of MPPH, a minor decrease (5.3 ± 1.3%) in CLPF was observed. Overall, these results indicate that, unlike compound I, compound II is incapable of directly contributing to the formation of the cross-link.

Stopped-Flow UV−Visible Characterization of Compounds I and III in KatG(M255I). Stopped-flow UV−visible spectroscopic methods were employed to detect the high valent iron−oxo compound I and oxyferrous compound III intermediates of KatG(M255I). For characterization of compound I, rapid mixing (2 ms) of a solution of ferric KatG(M255I) with 10 equiv of H_2O_2 yielded within 85 ms a new species [UV−visible spectrum, 407 (Soret, ϵ = 74 mM^{-1} cm^{-1}), 518, 560 (sh) nm] (Figure 8) whose spectral features matched neither those for compound II [UV−visible spectrum for WT KatG, 410 (Soret), 628 nm; UV−visible spectrum for KatG(Y229F), 417 (Soret), 531, 561 nm] nor those for compound III [UV−visible spectrum for WT KatG, 418 (Soret), 545, 580 nm; UV−visible spectrum for KatG(Y229F), 418 (Soret), 545, 581 nm] (Table 2). The spectral features, however, were consistent (with respect to λ_{max} and extinction) with the previously characterized compound I intermediates of *Synechocystis* PCC 6803 KatG(M275I) [UV−visible spectrum, 407 (Soret exhibits ~20% hypochromicity), ~522, ~570 (sh) nm] (*26*) and *Mtb* KatG(Y229F) [UV−visible spectrum, ~408 (Soret exhibits ~8% hypochromicity), ~520, ~555 (sh) nm]. On the basis of these spectral similarities, as well as the distinct hypochromicity of the Soret band, we assign this intermediate observed here as *Mtb* KatG(M255I) compound I. Values of k_{obs} for compound I formation were linearly dependent on H_2O_2 concentration (10−100-fold excess per heme), giving a bimolecular rate constant of (3.8 ± 0.3) × 10^5 M^{-1} s^{-1}. This rate is approximately 30-fold faster than that found for WT KatG (*39*), but ~10-fold slower than that found for KatG(Y229F) (*38*) (Table 2), suggesting that the presence of the cross-link does impact the rate of compound I formation, but not its spectroscopic properties.

Under these conditions of excess peroxide, the compound I intermediate was found to be unstable at pH 7.5 and 25 °C, and rapidly converted (3.7 ± 0.4 s^{-1}) in a H_2O_2 concentration-independent manner to a second intermediate whose spectral features [417 (Soret), 538, 578 nm] (Figure

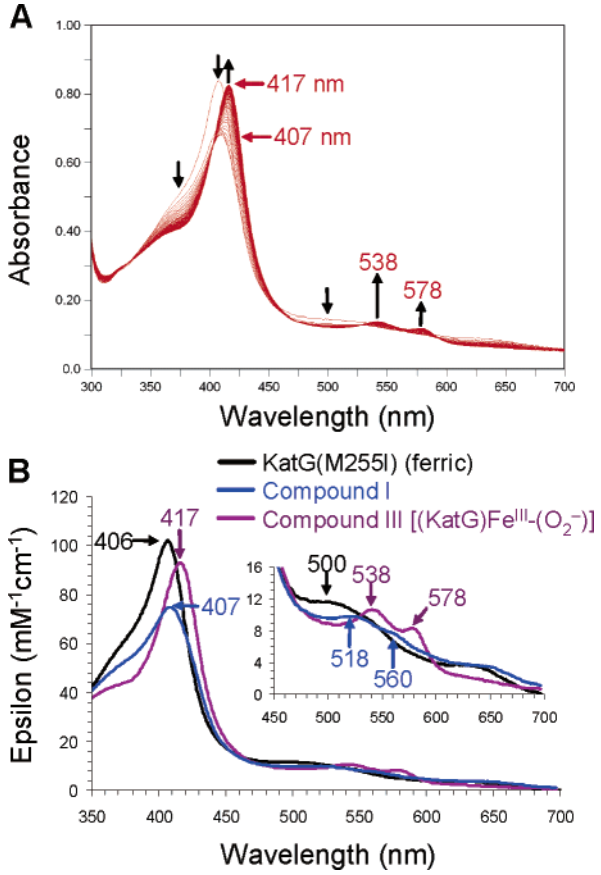

FIGURE 8: (A) Stopped-flow UV−visible spectroscopic monitoring of the reaction (300 scans, 6 s) between KatG(M255I) (10 μM) and a 10-fold excess of H_2O_2. See Experimental Procedures for details. (B) Calculated UV−visible spectra for both resting (black), compound I (blue), and compound III (purple) KatG(M255I). The rapid-scanning data from panel A were compiled and fitted to a double-exponential reaction model using the Specfit global analysis program.

8B) match well those previously assigned (*31*, *32*, *38*, *39*) to KatG compound III (Table 2). A similar conversion of compound I to compound III under conditions of excess peroxide has been noted for both *Mtb* KatG(Y229F) (*38*) and *Synechocystis* PCC 6803 KatG(Y249F) (*41*). The oxyferrous intermediate was also found to be unstable under these conditions, with either a slow decay (0.013 ± 0.001 s^{-1}) back to the resting enzyme at low H_2O_2 concentrations (100 μM) or bleaching of the compound III spectrum at high H_2O_2 concentrations (1−10 mM). At high concentrations of H_2O_2 (1000-fold excess), the reaction with KatG(M255I) proceeded at such an accelerated rate that compound I was formed within the mixing time of the stopped-flow apparatus.

Observation of the Oxoferryl Compound II [(KatG)(Por)-Fe^{IV}═O] Intermediate in KatG(M255I). In contrast to the observations of compounds I and III with excess hydrogen peroxide, stopped-flow rapid mixing of KatG(M255I) with 1 equiv of H_2O_2 revealed a completely new intermediate [UV−visible spectrum, 415 (Soret, ϵ = 82 mM^{-1} cm^{-1}), 531, 560 nm] (Figure 9) whose spectral features matched neither those of KatG(M255I) compound I nor those of compound III (vide supra, Table 2). The spectral features (λ_{max} and ϵ) match well those of the previously characterized oxoferryl-type [(KatG)(Por)Fe^{IV}═O] compound II intermediate of KatG(Y229F) [UV−visible spectrum, ~417 (Soret), ~531, ~561 nm] (*24*, *38*), with the compound II spectrum of *Synechocystis* PCC 6803 KatG(Y249F) [UV−visible spectrum, 418 (Soret), 530, 558 nm] (*28*), as well as for the classical oxoferryl compound II intermediates observed in HRP and other peroxidases (*42*). The value for k_{obs} for KatG-(M255I) oxoferryl compound II formation measured under these stoichiometric conditions was determined to be (1.4 ± 0.1) × 10^5 M^{-1} s^{-1}, similar to the rate observed for compound I formation (vide supra), and suggests that oxoferryl compound II is formed upon a very fast endogenous reduction of compound I, whose formation is rate-limiting.

The oxoferryl intermediate was found to be unstable under these conditions, converting (0.011 ± 0.001 s^{-1}) to a new species whose spectral features [408 (Soret), 556 (sh), 615 nm] (Figure 9B) matched those of (KatG$^{\bullet}$)(Por)Fe^{III}-OH compound II (vide infra) (Figure 10B). Decay of this species resulted in re-formation of the resting enzyme (0.006 ± 0.002 s^{-1}).

Observation of Compound II [(KatG$^{\bullet}$)(Por)Fe^{III}-OH] in KatG(M255I). Once a solution of ferric KatG(M255I) with MPPH had been rapidly mixed (2 ms) (Figure 10A), a new species was observed [UV−visible spectrum, 408 (Soret, ϵ = 110 mM^{-1} cm^{-1}), 556 (sh), 615 nm] (Figure 10B) whose spectral features did not match those of KatG(M255I) compound I, II (oxoferryl), or III (vide supra, Table 2). The spectral features, however, were highly consistent with those of the previously characterized (KatG$^{\bullet}$)(Por)Fe^{III}-OH compound II intermediates of WT KatG (*24*), KatG(R418L) (*31*), KatG(S315T) (*31*), *Synechocystis* PCC 6803 KatG (*43*), and *Anacystis nidulans* KatG (*44*). Values of k_{obs} for formation of this new species were linearly dependent on MPPH concentration (2.5−10-fold excess per heme), giving a bimolecular rate constant of (1.0 ± 0.2) × 10^4 M^{-1} s^{-1}, on a par with that determined for WT KatG under identical conditions (4.8 × 10^4 M^{-1} s^{-1}) (*24*). The intermediate was found to be unstable under these conditions, with a slow decay (0.004 s^{-1}) resulting in re-formation of the resting (ferric) enzyme, concomitant with a slight bleaching (~3%) of the heme Soret band. On the basis of these UV−visible spectroscopic observations and the known chemical reactivity of the MPPH oxidant (*40*, *45*), we assign the new species detected here as the (KatG$^{\bullet}$)(Por)Fe^{III}-OH compound II intermediate of *Mtb* KatG(M255I).

Reaction of KatG(M255I) with Peroxyacetic Acid. Stopped-flow mixing of a solution of ferric KatG(M255I) with 1 equiv of PAA led to the formation of a new species [UV−visible spectrum, 409 (Soret, ϵ = 108 mM^{-1} cm^{-1}), 556, 615 nm] (Figure S2) whose spectral features matched those of (KatG$^{\bullet}$)(Por)Fe^{III}-OH compound II as generated with MPPH. The bimolecular rate constant of (9.2 ± 0.4) × 10^4 M^{-1} s^{-1} was determined for the single concentration of 10 μM PAA. The compound II intermediate was found to be unstable under these conditions, with a slow decay (0.006 ± 0.001 s^{-1}) resulting in re-formation of the resting (ferric) enzyme. Bleaching of the heme Soret band was not observed under these conditions.

At higher PAA concentrations (4−20-fold excess) (Figure S3), the first observed intermediate was that of oxoferryl compound II [UV−visible spectrum, 415 (Soret, ϵ = 82 mM^{-1} cm^{-1}), 531, 560 nm]. Values of k_{obs} for formation of this new species were linearly dependent on PAA concentration (4−20-fold excess per heme), giving a bimolecular rate

Table 2: UV−Visible Spectroscopic Data and Kinetic Parameters for the Oxidized Intermediates of KatG(M255I), WT KatG, and KatG(Y229F)

	λ_{max} (mM^{-1} cm^{-1}) (ϵ)	k_{obs} (M^{-1} s^{-1})	ref
KatG(M255I)			
ferric (resting)	406 (101), 500, 540, 620	not applicable	*a*
compound I	407 (74), 518, 560 (sh)	$(3.8 \pm 0.3) \times 10^5$	*a*
compound II − (KatG•)(Por)Fe^{III}-OH	408 (110), 500, 556, 615	$(1.0 \pm 0.2) \times 10^4$ [b]	*a*
compound II − (KatG)(Por)Fe^{IV}=O	415 (82), 531, 560	$(1.4 \pm 0.1) \times 10^5$ [c] $(1.8 \pm 0.4) \times 10^4$ [d]	*a*
compound III	417 (94), 538, 578	3.7 ± 0.4 s^{-1} [e]	*a*
WT KatG			
compound I	411, 550, 590, 655	1.21×10^4 [e]	*39*
compound II − (KatG•)(Por)Fe^{III}-OH	410, 628	$(4.8 \pm 0.4) \times 10^4$	*24*
compound III	418, 545, 580	$>10^9$	*31*
KatG(Y229F)			
compound I	408, ~520, ~555 (sh)	4×10^6	*38*
compound II − (KatG)(Por)Fe^{IV}=O	417, 531, 561	$(5.8 \pm 0.7) \times 10^6$	*24*
compound III	418, 545, 581	$(9.2 \pm 0.2) \times 10^5$	*31*

[a] From this work. [b] When formed with MPPH. [c] When formed with 1 equiv of H_2O_2. [d] When formed with PAA. [e] Measurement of compound I to compound III conversion.

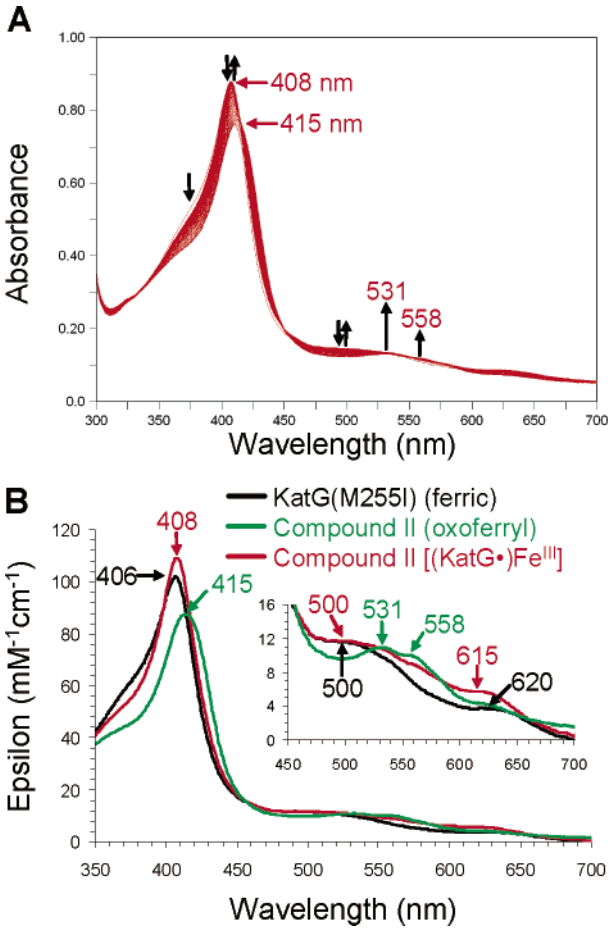

FIGURE 9: (A) Stopped-flow UV−visible spectroscopic monitoring of the reaction (300 scans, 60 s) between KatG(M255I) (10 μM) and 1 equiv of H_2O_2. See Experimental Procedures for details. (B) Calculated UV−visible spectra for resting (black) and oxoferryl [(KatG)(Por)Fe^{IV}=O] compound II KatG(M255I) (green). The rapid-scanning data from panel A were compiled and fitted to a double-exponential reaction model using the Specfit global analysis program.

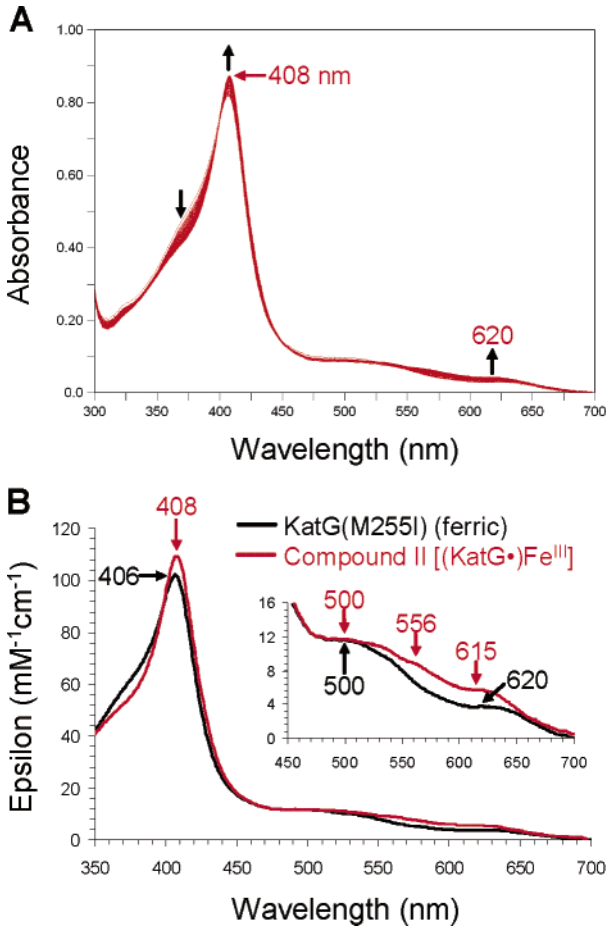

FIGURE 10: (A) Stopped-flow UV−visible spectroscopic monitoring of the reaction (300 scans, 6 s) between KatG(M255I) (10 μM) and a 10-fold excess of MPPH. See Experimental Procedures for details. (B) Calculated UV−visible spectra for both resting (black) and (KatG•)(Por)Fe^{III}-OH compound II KatG(M255I) (red). The rapid-scanning data from panel A were compiled and fitted to a single-exponential reaction model using the Specfit global analysis program.

constant of $(1.8 \pm 0.4) \times 10^4$ M^{-1} s^{-1}, similar to the rate of compound I formation (vide supra), which again suggests that compound II is derived from a fast endogenous reduction of compound I. The oxoferryl species was transiently stable under these conditions, slowly converting (0.051 ± 0.003 s^{-1}) to (KatG•)(Por)Fe^{III}-OH compound II [408 (Soret), 558 (sh), 615 nm] (Figure S3). Decay of this species resulted in re-formation of the resting enzyme with minor bleaching of the heme Soret band at the higher peroxide concentrations.

Stoichiometric Reaction of WT KatG with H_2O_2 or PAA As Revealed by Stopped-Flow UV−Visible Spectroscopy. Once a solution of ferric WT KatG with 1 equiv of either

H_2O_2 (Figure S4) or PAA (Figure S5) had been rapidly mixed (2 ms), a new species was observed [UV−visible spectrum, 410 (Soret, $\epsilon = 110$ mM^{-1} cm^{-1}), 628 nm] whose spectral features matched those previously (*24*) described for WT KatG compound II, (KatG$^{\bullet}$)(Por)Fe^{III}-OH, generated with MPPH (Table 2). The bimolecular rate constants of $(7.1 \pm 0.3) \times 10^5$ and $(4.8 \pm 0.8) \times 10^5$ M^{-1} s^{-1} were determined for a single concentration (10 μM) of H_2O_2 and PAA, respectively. The intermediate was found to be unstable under these conditions, with a slow decay (0.003 ± 0.001 s^{-1}) resulting in re-formation of the resting (ferric) enzyme. Bleaching of the heme Soret band was not observed under these conditions.

DISCUSSION

In our previous work in deciphering the mechanism of Met−Tyr−Trp cross-link formation and its role in *Mtb* KatG catalysis, we focused on WT KatG and KatG(Y229F), a mutant in which no cross-link could be formed (*24*). While we gained much insight into overall Met−Tyr−Trp cross-link formation, questions still remained with regard to formation of the individual bonds (i.e., Tyr−Trp and Met−Tyr), as well as the putative intermediates proposed to form along the reaction pathway. To address these and other relevant issues, we have studied the mutant KatG(M255I), whose Met → Ile substitution leads to only a Tyr−Trp cross-link, thus allowing us to deconvolute the effect of this individual component on enzyme catalysis and spectroscopy from that of the entire Met−Tyr−Trp cross-link. Differences in reactivity between Tyr−Trp and Met−Tyr−Trp cross-link-containing enzymes can also shed light on the contribution of the Met−Tyr bond.

We employed tryptic digestion of KatG in combination with high-pressure liquid chromatography and mass spectrometry to identify the presence of a peptide fragment containing the Tyr−Trp cross-link (CLPF). A similar approach was taken in identifying the Met−Try−Trp cross-link in WT KatG, with isolation of the CLPF by HPLC prior to mass spectrometric characterization allowing for quantification as well as confirmation of its presence. Identification of a candidate for the Tyr−Trp CLPF was simplified by comparison of the HPLC chromatograms obtained for the tryptic digest of KatG(M255I) to those of KatG(Y229F), which has been shown to lack any CLPF as a consequence of its Tyr → Phe mutation. Several peptide fragments which clustered together in the former but not latter digest exhibited unusual UV−visible spectra for polypeptides. The major peptide fragment displayed large bathochromic shifts of the protein absorption bands [$\lambda_{max} = 252$ (sh) and 296 nm], similar to the UV−visible spectrum observed for the CLPF of WT KatG, and highly suggestive of the presence of a cross-link in KatG(M255I). Surprisingly, the minor isolated peptide fragments exhibited even larger bathochromic shifts [$\lambda_{max} = 252$ (sh), 308, and 320 nm], suggesting two possible structures of the Tyr−Trp CLPFs in KatG(M255I).

Isolation of these CLPF candidates, and subsequent characterization by mass spectrometry, conclusively demonstrated the existence of the Tyr−Trp cross-link in KatG(M255I). The major CLPF was found to contain the unmodified Tyr−Trp cross-link (Figure 4B), whose structure was confirmed by CID and MS/MS/MS analyses. For the remaining minor CLPFs, the unusual observed masses are all derived from a species whose mass is 2 Da lower than that of the Tyr−Trp CLPF, with the loss in mass centered on either Trp107 or Tyr229 (or both), and not on the other residues comprising the CLPF. We propose that the structure of this intermediate is best represented by the ^{QL}Tyr−Trp quinone-like species (Figure 4C), and we have previously proposed that this intermediate is formed in the autocatalytic mechanism of Met−Tyr−Trp cross-link formation (vide infra).

Overexpression of apo-KatG(M255I), followed by in vitro reconstitution with heme in the absence of exogenously added peroxide, yielded ^{R}KatG(M255I), a holoenzyme lacking the Tyr−Trp cross-link normally found in the recombinant enzyme. This allowed for the study of cross-link formation under oxidizing conditions that proceed through either compound I (PAA) or compound II (MPPH) intermediates. Incubation of ^{R}KatG(M255I) with peroxyacetic acid (0−10 equiv/heme) revealed a reaction stoichiometry (for full Tyr−Trp CLPF formation) of 3.5 equiv of PAA per KatG (monomer). Higher stoichiometries led to loss of the CLPF, a behavior that was not observed for the Met−Tyr−Trp cross-link-containing CLPF in WT KatG, and suggests that further oxidation of the Tyr−Trp cross-link beyond the ^{QL}Tyr−Trp intermediate results in a species that is too unstable for isolation. The finding that Tyr−Trp CLPF formation (one cross-link bond) is most prominent after the addition of ∼3.5 equiv of PAA is in good agreement with the midpoint value of 3 equiv determined for Met−Tyr−Trp CLPF formation (two cross-link bonds present, 6 equiv of PAA).

Given that peroxyacetic acid is a two-electron oxidant, the disparity between the seven oxidizing equivalents needed for what is formally a two-electron oxidation (formation of the single covalent bond in the Tyr−Trp cross-link) leads us to conclude that under the conditions studied, cross-link formation is only ∼30% efficient. In WT KatG, cross-link formation was similarly inefficient (∼33%). We suggest that additional oxidizing equivalents may generate protein radicals outside the heme active site, as has been previously observed for both *Mtb* (*38*, *46*, *47*) and *Synechocystis* PCC 6803 (*26*, *48*) KatGs. Alternatively, higher efficiency may occur in vivo in the presence of the bound substrate, or by the intervention of a cellular assembly system.

Incubation of ^{R}KatG(M255I) with a large excess of MPPH, which preferentially oxidizes KatG to compound II over compound I (as demonstrated by stopped-flow UV−visible spectroscopic studies), yielded no increase in the level of Tyr−Trp CLPFs detected, similar to what was previously observed for the Met−Tyr−Trp cross-link in WT KatG (*24*). This suggests that both oxidizing equivalents must be present simultaneously to achieve bond formation. In the only other example of a Tyr−Trp bond, C*c*P(H52Y) (*49*), the histidine → tyrosine mutation allows for the formation of a C−N bond (as opposed to the C−C bond in *Mtb* KatG) between the indolic N (Nϵ1) of Trp51 and Cϵ1 of Tyr52. Poulos and co-workers argue that given the short lifetimes of protein radicals, two sequential one-electron oxidations by two compound I intermediates (resulting from two enzyme turnovers) yielding the Tyr−Trp bond are unlikely to occur in C*c*P(H52Y) (*49*). Rather, they contend that any mechanism for bond formation between two protein side chains must

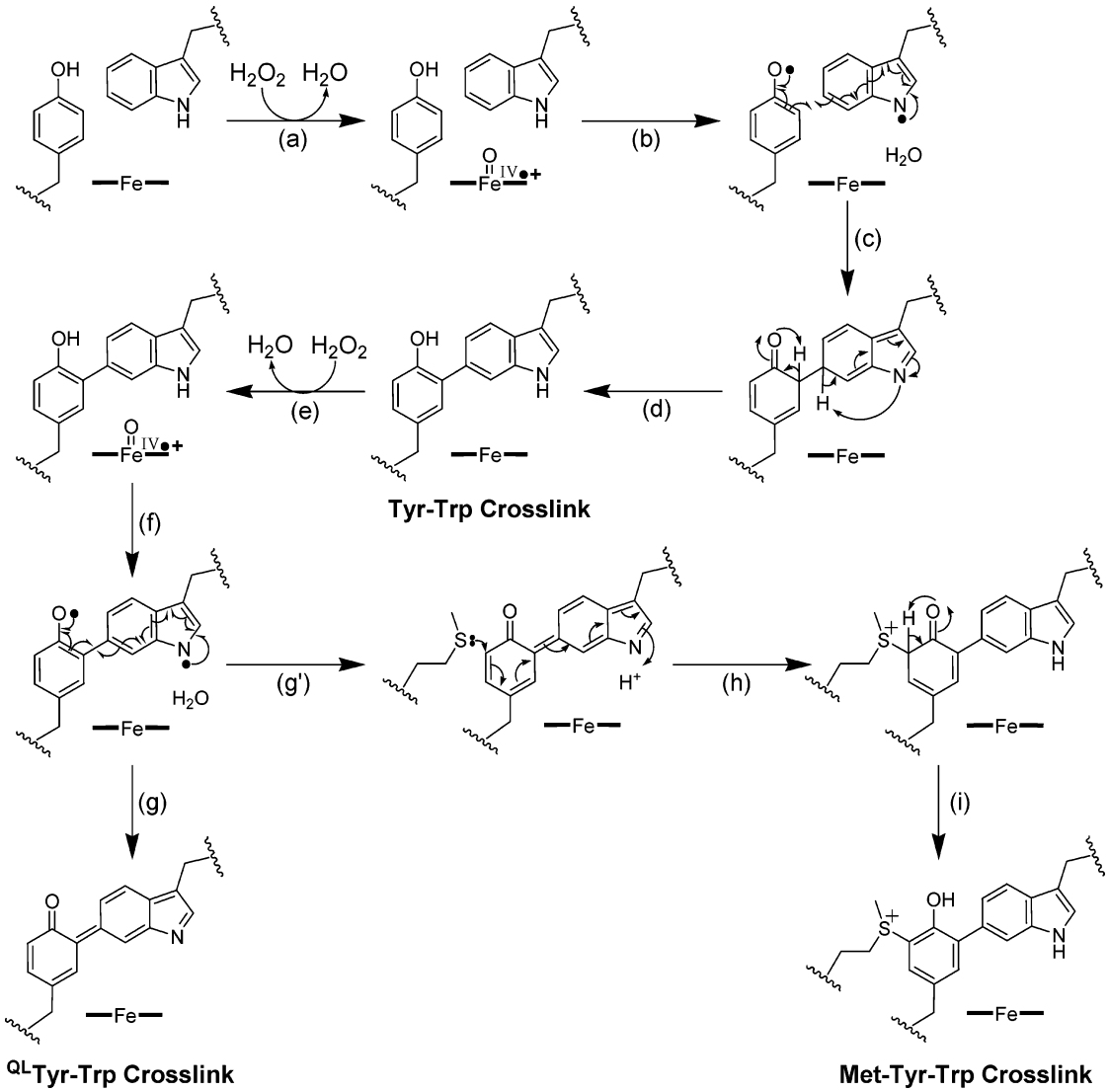

FIGURE 11: Proposed mechanism for the formation of the Tyr−Trp and Met−Tyr−Trp cross-links in KatG(M255I) and WT KatG, respectively. All oxidation states are ferric except where indicated.

support concurrent radical formation on both protein residues, and our data which demonstrate the lack of Tyr−Trp CLPF formation derived from KatG(M255I) compound II (one oxidizing equivalent above the resting state) support this notion.

On the basis of the results given above, we propose the following mechanism for Tyr−Trp bond formation in KatG(M255I): Formation of compound I (Figure 11, step a) either by a peracid (in vitro) or by hydrogen peroxide (in vivo) leads to oxidation of both Tyr229 and Trp107 (step b). From the crystal structure of *Mtb* WT KatG, the indole ring of Trp107 is nearly coplanar and stacked above the pyrrole B ring of the heme cofactor at a distance of 3.53 Å (3.4 Å in *Burkholderia pseudomallei* KatG), while Tyr229 is also within ~5.4 Å (Cδ^2 to pyrrole A) of the heme periphery (*11*). Both of these redox active residues are therefore within the threshold for long-range electron transfer (*50*, *51*) and are capable of being oxidized by compound I with concomitant formation of Trp107$^\bullet$ and Tyr229$^\bullet$. As both protein radicals are formed simultaneously from a single turnover event, their lifetimes are not an issue, and coupling of the two radicals (step c) results in formation of the Tyr−Trp bond (step d) between Cη2 of Trp107 and Cϵ1 of Tyr229. Formation of a second compound I intermediate (step e) results in further oxidation of the Tyr−Trp cross-link (steps f), leading to the quinone-like intermediate ^{QL}Tyr−Trp (step g), as suggested by the mass spectrometric results. In KatG(M255I), further reaction with this oxidized species is not possible. However, in WT KatG, nucleophilic attack of the sulfur atom of Met255 on ^{QL}Tyr−Trp (step g′) occurs, resulting in formation of a bond between Cϵ2 of Tyr229 and Sδ of Met255 (steps h and i), yielding the Met−Tyr−Trp cross-link. This proposed mechanism accounts for the study by Obinger and co-workers who found that the mutation of the tryptophan residue did not yield any Met−Tyr−Trp cross-link in *Synechocystis* PCC 6803 KatG (*27*). Thus, a sequential process of bond formation between Tyr229 and Trp107, followed by Tyr229 and Met255, is proposed.

The UV−visible spectral features of compounds I and III do not vary significantly among KatG(M255I), WT KatG, and KatG(Y229F), suggesting that the presence or absence of either the Tyr−Trp or Met−Tyr−Trp cross-link does not greatly alter the spectroscopic properties of these intermediates despite the strong influence on enzymatic activity. The UV−visible spectrum of compound II does, however, vary considerably among the three enzymes, and we have previ-

ously reported (*24*) that the spectral dependency of compound II correlates to enzyme function: WT KatG (Met−Tyr−Trp cross-link present) has both catalase and peroxidase activities, and the compound II species exhibits spectral features that are catalase-peroxidase-like (slight hyperchromicity of the Soret band, with little to no shift observed vs the ferric resting enzyme, and the presence of an ∼625 nm feature). On the other hand, KatG(Y229F) (Met−Tyr−Trp cross-link absent) has only peroxidase activity, and exhibits the classical peroxidase-like oxoferryl compound II spectrum (red shift in the Soret band by ∼10 nm, as well as prominent ∼530 and 560 nm features). In this study, we show that KatG(M255I) (Tyr−Trp cross-link present) exhibits both compound II spectra yet retains only peroxidase activity. Therefore, simply exhibiting a specific compound II spectrum is not enough to determine whether catalase activity is observed; rather, the absence of any oxoferryl spectrum appears to be the primary requisite.

The spectral differences between the two compound II intermediates may be explained in light of two isoelectronic structures for a $1e^-$ oxidized state of KatG, (KatG)(Por)-Fe^{IV}═oxo or (KatG$^\bullet$)(Por)Fe^{III}-OH, where KatG$^\bullet$ represents a protein radical not electronically coupled to the heme (*42*, *52*, *53*). The former represents the "classical" oxoferryl species of the peroxidases, whereas the latter represents the catalase-peroxidase compound II, whose structure has been suggested to have an absorption spectrum only slightly perturbed from that of the resting enzyme (*42*−*44*). Both of these compound II species can be formed directly, but only the oxoferryl species (KatG)(Por)Fe^{IV}═oxo interconverts to that of the protein radical (KatG$^\bullet$)(Por)Fe^{III}-OH, suggesting that protein side chain-based reduction of the oxoferryl intermediate is favorable.

The question of why compound II is different in the catalase-peroxidases versus the monofunctional peroxidases arises. What could the mechanistic advantage of (KatG$^\bullet$)-(Por)Fe^{III}-OH be over (KatG)(Por)Fe^{IV}═O? The latter species is inactive with respect to catalase activity (formation of compound III ensuing upon reaction with a second equivalent of H_2O_2). However, we have previously suggested that the former may still possess catalase activity (*24*). In (KatG$^\bullet$)-(Por)Fe^{III}-OH, the heme is essentially in the resting state (protonation of the axial hydroxide ligand to water by the extensive H-bonding network in KatG upon peroxide binding notwithstanding), and therefore capable of reducing H_2O_2 to yield compound I (the first step common to both catalase and peroxidase cycles). Thus, by transferring the oxidizing equivalent to the protein, an oxoferryl intermediate can be prevented and catalase activity is maintained. This possibility would be unique only to the KatGs, as preventing compound II from forming is a conundrum which only a bifunctional enzyme employing a common intermediate (i.e., a catalase-peroxidase using compound I in both catalytic mechanisms) must address. Catalases themselves lack peroxidase−substrate binding sites, and are thus unlikely to undergo reduction of compound I to compound II by an exogenous electron source, a process which the KatGs must overcome. On the other hand, peroxidases are able to perform two sequential one-electron oxidations, and the presence of a relatively stable classical oxoferryl compound II in the absence of a second reducing substrate would inhibit any subsequent catalase activity in a KatG. Accordingly, the function of the cross-link may be to protect the catalase-peroxidase by promoting oxoferryl reduction with concomitant oxidation of a protein side chain, thereby ensuring that the heme cofactor remains in a catalytically competent state for both enzyme activities during turnover.

One interesting possibility is that WT KatG accomplishes this by promoting a rapid two-electron reduction of compound I. Support for this is provided by stopped-flow UV−visible spectroscopic studies in which KatG is reacted with a stoichiometric equivalent of H_2O_2 (identical results were also obtained with 1 equiv of PAA). Under such "single-turnover" conditions, catalase activity is not possible, allowing for comparisons to the wild-type enzyme. For KatG(Y229F), reaction with 1 equiv of H_2O_2 led to formation of the oxoferryl compound II intermediate (*38*), presumably due to initial reduction of compound I by Trp107. Similarly, in the 1:1 reaction of KatG(M255I) with H_2O_2, the oxoferryl intermediate is observed first, most likely due to a rapid reduction of compound I by the Tyr−Trp cross-link. However, in a departure from what is observed with KatG-(Y229F), oxoferryl compound II slowly converts to (KatG$^\bullet$)-(Por)Fe^{III}-OH compound II, and we suggest that this second reducing equivalent is also donated by the Tyr−Trp cross-link. This two-electron oxidation would yield the ^{QL}Tyr−Trp species as observed in our mass spectrometric studies, and this species is suggested to be a key intermediate in the formation of the Met−Tyr−Trp cross-link in WT KatG. For the WT enzyme, only (KatG$^\bullet$)(Por)Fe^{III}-OH compound II is observed upon reaction with a stoichiometric amount of H_2O_2, suggesting that a two-electron reduction of WT KatG compound I readily occurs. We propose that the first electron is provided by the Met−Tyr−Trp cross-link. This is similar to KatG(Y229F) or KatG(M255I), where either Trp107 or the Tyr−Trp cross-link, respectively, reduces compound I to the catalase-inactivating oxoferryl compound II. However, unlike these two catalase-deficient enzymes, WT KatG rapidly reduces oxoferryl compound II to (KatG$^\bullet$)(Por)Fe^{III}-OH compound II, thereby maintaining catalase activity.

With regard to the origin of the second electron donor in WT KatG, several possibilities exist. Mutagenesis studies (*48*) in conjunction with EPR spectroscopy on *Synechocystis* PCC 6803 *KatG* suggest it may be Trp106 (Trp91 in *Mtb*). Trp91 is part of an integral H-bonding network that includes Trp107 of the Met−Tyr−Trp cross-link, several waters, the heme propionate arm, and the catalytically important distal histidine (His108) and arginine (R104) residues, making it a good candidate for reducing oxoferryl compound II in *Mtb* KatG. On the other hand, Magliozzo and co-workers have found evidence for a tyrosyl radical in both WT KatG (*54*) and KatG(Y229F) (*38*), with mutagenesis studies suggesting that Tyr353 may be the specific residue that is involved (*46*). In either case, however, with two oxidizing equivalents stored on the protein, formation of the oxoferryl intermediate is circumvented, thereby preventing this catalase-inactivating species.

While the Met−Tyr−Trp cross-link may be capable of acting as a two-electron donor, thereby forming a ^{QL}Met−Tyr−Trp species (similar to ^{QL}Tyr−Trp, but possessing the additional Met−Tyr cross-link), we disfavor this possibility for several reasons. First, the presence of the sulfonium ion likely raises the reduction potential of the cross-link, making it progressively harder for the cross-link to donate electrons.

Second, unlike the ^{QL}Tyr−Trp CLPF, we were unable to identify the corresponding ^{QL}Met−Tyr−Trp CLPF by mass spectrometry. Finally, the stability afforded by the ^{QL}Met−Tyr−Trp species would most likely limit its ability to function in the peroxidase cycle in two independent one-electron steps. Thus, it appears that the role of the sulfonium ion may be to prevent ^{QL}Met−Tyr−Trp cross-link formation, thereby promoting oxoferryl compound II reduction from one of the aforementioned redox active protein side chains.

Other plausible explanations that could account for the two different compound II spectra exist. Protein environment strongly influences the spectral properties of the heme prosthetic group, and mutations which affect the cross-link are expected to have a cascade effect on the overall protein architecture of the active site: the side chain of Tyr229 is covalently bound to the side chain of Trp107, which itself is part of the aforementioned active site H-bonding network. Such changes in the active site may affect π-stacking interactions between Trp107 and the heme, influence the geometry of the heme in its binding pocket, weaken or strengthen the iron−oxo bond, or disrupt distal side hydrogen bonding networks, all of which could in turn influence the electronic absorption spectrum of compound II. In support of the latter, several KatG mutations have been shown to disrupt active site hydrogen bonding networks (*25*, *55*, *56*), and it is conceivable that such an alteration in H-bonding to the oxo moiety of compound II may alter its spectroscopic signature.

We have been able to show that the Tyr−Trp cross-link in KatG(M255I) forms autocatalytically, that its presence alters the spectral features of KatG compound II which may form during catalysis, and that this correlates well to changes in enzymatic function, particularly catalase activity. An oxidized form of the Tyr−Trp cross-link has been observed which supports our previous mechanism for Met−Tyr−Trp cross-link formation. In addition, we suggest a mechanism of protection against catalase inactivation by oxoferryl compound II which is predicated solely upon the Met−Tyr−Trp cross-link, establishing a molecular basis for the cross-link which correlates with catalase activity. It is clear from this work that an enzyme structure−spectroscopy−activity relationship is readily observed in the catalase-peroxidases which is solely attributed to the presence of the Tyr−Trp and Met−Tyr−Trp cross-links.

ACKNOWLEDGMENT

We acknowledge the Colorado State University (NIAID Contract N01 AI-75320) for supplying the KatG-encoding plasmid pMRLB11. We thank Jessica Tenenbaum for stimulating discussions on H-bonding to iron−oxo moieties.

SUPPORTING INFORMATION AVAILABLE

UV−visible spectroscopic data and analysis for KatG(M255I), WT KatG, and KatG(Y229F) (Table S1); UV−visible spectra of apo-KatG(M255I) before and after heme reconstitution [as ^{R}KatG(M255I)] (Figure S1); stopped-flow UV−visible spectra and analysis of the reaction of 1 and 4 equiv of PAA (Figures S2 and S3, respectively) with KatG(M255I); and stopped-flow UV−visible spectra and analysis for the reaction between WT KatG and 1 equiv of H_2O_2 (Figure S4) or PAA (Figure S5). This material is available free of charge via the Internet at http://pubs.acs.org.

REFERENCES

1. Welinder, K. G. (1992) Superfamily of Plant, Fungal, and Bacterial Peroxidases, *Curr. Opin. Struct. Biol. 2*, 388−393.
2. Welinder, K. G. (1991) Bacterial Catalase-Peroxidases Are Gene Duplicated Members of the Plant Peroxidase Superfamily, *Biochim. Biophys. Acta 1080*, 215−220.
3. Zamocky, M., Regelsberger, G., Jakopitsch, C., and Obinger, C. (2001) The molecular peculiarities of catalase-peroxidases, *FEBS Lett. 492*, 177−182.
4. Zabinski, R. F., and Blanchard, J. S. (1997) The Requirement for Manganese and Oxygen in the Isoniazid-Dependent Inactivation of *Mycobacterium tuberculosis* Enoyl Reductase, *J. Am. Chem. Soc. 119*, 2331−2332.
5. Magliozzo, R. S., and Marcinkeviciene, J. A. (1997) The role of Mn(II)-peroxidase activity of mycobacterial catalase-peroxidase in activation of the antibiotic isoniazid, *J. Biol. Chem. 272*, 8867−8870.
6. Magliozzo, R. S., and Marcinkeviciene, J. A. (1996) Evidence for Isoniazid Oxidation by Oxyferrous Mycobacterial Catalase-Peroxidase, *J. Am. Chem. Soc. 118*, 11303−11304.
7. Wengenack, N. L., Jensen, M. P., Rusnak, F., and Stern, M. K. (1999) *Mycobacterium tuberculosis* KatG is a Peroxynitritase, *Biochem. Biophys. Res. Commun. 256*, 485−487.
8. Yamada, Y., Fujiwara, T., Sato, T., Igarashi, N., and Tanaka, N. (2002) The 2.0 Å Crystal Structure of Catalase-Peroxidase from *Haloarcula marismortui*, *Nat. Struct. Biol. 9*, 691−695.
9. Carpena, X., Loprasert, S., Mongkolsuk, S., Switala, J., Loewen, P. C., and Fita, I. (2003) Catalase-peroxidase KatG of *Burkholderia pseudomallei* at 1.7 Å resolution, *J. Mol. Biol. 327*, 475−489.
10. Wada, K., Tada, T., Nakamura, Y., Kinoshita, T., Tamoi, M., Shigeoka, S., and Nishimura, K. (2002) Crystallization and preliminary X-ray diffraction studies of catalase-peroxidase from *Synechococcus* PCC 7942, *Acta Crystallogr. D58*, 157−159.
11. Bertrand, T., Eady, N. A. J., Jones, J. N., Jesmin, Nagy, J. M., Jamart-Grégoire, B., Raven, E. L., and Brown, K. A. (2004) Crystal Structure of *Mycobacterium tuberculosis* Catalase-Peroxidase, *J. Biol. Chem. 279*, 38991−38999.
12. Ostermeier, C., Harrenga, A., Ermler, U., and Michel, H. (1997) Structure at 2.7 Å resolution of the *Paracoccus denitrificans* two-subunit cytochrome *c* oxidase complexed with an antibody FV fragment, *Proc. Natl. Acad. Sci. U.S.A. 94*, 10547−10553.
13. Yoshikawa, S., Shinzawa-Itoh, K., Nakashima, R., Yaono, R., Yamashita, E., Inoue, N., Yao, M., Fei, M. J., Libeu, C. P., Mizushima, T., Yamaguchi, H., Tomizaki, T., and Tsukihara, T. (1998) Redox-coupled crystal structural changes in bovine heart cytochrome *c* oxidase, *Science 280*, 1723−1729.
14. Buse, G., Soulimane, T., Dewor, M., Meyer, H. E., and Bluggel, M. (1999) Evidence for a copper-coordinated histidine-tyrosine cross-link in the active site of cytochrome oxidase, *Protein Sci. 8*, 985−990.
15. Bravo, J., Fita, I., Ferrer, J. C., Ens, W., Hillar, A., Switala, J., and Loewen, P. C. (1997) Identification of a novel bond between a histidine and the essential tyrosine in catalase HPII of *Escherichia coli*, *Protein Sci. 6*, 1016−1023.
16. Ito, N., Phillips, S. E., Yadav, K. D., and Knowles, P. F. (1994) Crystal structure of a free radical enzyme, galactose oxidase, *J. Mol. Biol. 238*, 794−814.
17. Ito, N., Phillips, S. E., Stevens, C., Ogel, Z. B., McPherson, M. J., Keen, J. N., Yadav, K. D., and Knowles, P. F. (1991) Novel thioether bond revealed by a 1.7 Å crystal structure of galactose oxidase, *Nature 350*, 87−90.
18. Diaz, A., Horjales, E., Rudino-Pinera, E., Arreola, R., and Hansberg, W. (2004) Unusual Cys-Tyr covalent bond in a large catalase, *J. Mol. Biol. 342*, 971−985.
19. Parsons, M. R., Convery, M. A., Wilmot, C. M., Yadav, K. D., Blakeley, V., Corner, A. S., Phillips, S. E., McPherson, M. J., and Knowles, P. F. (1995) Crystal structure of a quinoenzyme: Copper amine oxidase of *Escherichia coli* at 2 Å resolution, *Structure 3*, 1171−1184.
20. Proshlyakov, D. A., Pressler, M. A., DeMaso, C., Leykam, J. F., DeWitt, D. L., and Babcock, G. T. (2000) Oxygen activation and reduction in respiration: involvement of redox-active tyrosine 244, *Science 290*, 1588−1591.

21. Whittaker, J. W. (2005) The radical chemistry of galactose oxidase, *Arch. Biochem. Biophys. 433*, 227−239.
22. Mate, M. J., Sevinc, M. S., Hu, B., Bujons, J., Bravo, J., Switala, J., Ens, W., Loewen, P. C., and Fita, I. (1999) Mutants that alter the covalent structure of catalase hydroperoxidase II from *Escherichia coli*, *J. Biol. Chem. 274*, 27717−27725.
23. Rogers, M. S., and Dooley, D. M. (2003) Copper-tyrosyl radical enzymes, *Curr. Opin. Chem. Biol. 7*, 189−196.
24. Ghiladi, R. A., Knudsen, G. M., Medzihradszky, K. F., and Ortiz de Montellano, P. R. (2005) The Met-Tyr-Trp crosslink in *Mycobacterium tuberculosis* catalase-peroxidase (KatG): Autocatalytic formation and effect on enzyme catalysis and spectroscopic properties, *J. Biol. Chem. 280*, 22651−22663.
25. Santoni, E., Jakopitsch, C., Obinger, C., and Smulevich, G. (2004) Manipulating the covalent link between distal side tryptophan, tyrosine, and methionine in catalase-peroxidases: An electronic absorption and resonance Raman study, *Biopolymers 74*, 46−50.
26. Jakopitsch, C., Ivancich, A., Schmuckenschlager, F., Wanasinghe, A., Poltl, G., Furtmuller, P. G., Ruker, F., and Obinger, C. (2004) Influence of the unusual covalent adduct on the kinetics and formation of radical intermediates in synechocystis catalase peroxidase: A stopped-flow and EPR characterization of the Met275, Tyr249, and Arg439 variants, *J. Biol. Chem. 279*, 46082−46095.
27. Jakopitsch, C., Kolarich, D., Petutschnig, G., Furtmuller, P. G., and Obinger, C. (2003) Distal side tryptophan, tyrosine and methionine in catalase-peroxidases are covalently linked in solution, *FEBS Lett. 552*, 135−140.
28. Jakopitsch, C., Auer, M., Ivancich, A., Ruker, F., Furtmuller, P. G., and Obinger, C. (2003) Total conversion of bifunctional catalase-peroxidase (KatG) to monofunctional peroxidase by exchange of a conserved distal side tyrosine, *J. Biol. Chem. 278*, 20185−20191.
29. Foster, T. L., and Caradonna, J. P. (2003) Fe^{2+}-Catalyzed Heterolytic RO−OH Bond Cleavage and Substrate Oxidation: A Functional Synthetic Non-Heme Iron Monooxygenase System, *J. Am. Chem. Soc. 125*, 3678−3679.
30. Hiatt, R. R., and Strachan, W. M. J. (1963) The Effect of Structure on the Thermal Stability of Hydroperoxides, *J. Org. Chem. 28*, 1893−1894.
31. Ghiladi, R. A., Medzihradszky, K. F., Rusnak, F. M., and Ortiz de Montellano, P. R. (2005) Correlation Between Isoniazid Resistance and Superoxide Reactivity in *Mycobacterium tuberculosis* KatG, *J. Am. Chem. Soc. 127*, 13428−13442.
32. Ghiladi, R. A., Cabelli, D. E., and Ortiz de Montellano, P. R. (2004) Superoxide reactivity of KatG: Insights into isoniazid resistance pathways in TB, *J. Am. Chem. Soc. 126*, 4772−4773.
33. Falk, J. E. (1964) in *Porphyrins and Metalloporphyrins: Their General, Physical, and Coordination Chemistry and Laboratory Methods*, pp 181−188, Elsevier, New York.
34. Fuhrhop, J. H., and Smith, K. M. (1975) in *Porphyrins and Metalloporphyrins* (Smith, K. M., Ed.) pp 804−807, Elsevier, New York.
35. Chouchane, S., Girotto, S., Kapetanaki, S., Schelvis, J. P., Yu, S., and Magliozzo, R. S. (2003) Analysis of heme structural heterogeneity in *Mycobacterium tuberculosis* catalase-peroxidase (KatG), *J. Biol. Chem. 278*, 8154−8162.
36. Nicholls, P., Fita, I., and Loewen, P. (2001) in *Advances in Inorganic Chemistry: Heme-Fe Proteins* (Sykes, A. G., and Mauk, G., Eds.) pp 51−106, Academic Press, San Diego.
37. Mate, M. J., Murshudov, G., Bravo, J., Melik-Adamyan, W., Loewen, P. C., and Fita, I. (2001) in *Handbook of Metalloproteins* (Messerschmidt, A., Huber, R., Poulos, T. L., and Weighardt, K., Eds.) pp 486−502, John Wiley & Sons, Chichester, U.K.
38. Yu, S., Girotto, S., Zhao, X., and Magliozzo, R. S. (2003) Rapid formation of compound II and a tyrosyl radical in the Y229F mutant of *Mycobacterium tuberculosis* catalase-peroxidase disrupts catalase but not peroxidase function, *J. Biol. Chem. 278*, 44121−44127.
39. Chouchane, S., Lippai, I., and Magliozzo, R. S. (2000) Catalase-peroxidase (*Mycobacterium tuberculosis* KatG) catalysis and isoniazid activation, *Biochemistry 39*, 9975−9983.
40. Nam, W., Han, H. J., Oh, S.-Y., Lee, Y. J., Choi, M.-H., Han, S.-Y., Kim, C., Woo, S. K., and Shin, W. (2000) New Insights into the Mechanisms of O−O Bond Cleavage of Hydrogen Peroxide and *tert*-Alkyl Hydroperoxides by Iron(III) Porphyrin Complexes, *J. Am. Chem. Soc. 122*, 8677−8684.
41. Jakopitsch, C., Wanasinghe, A., Jantschko, W., Furtmueller, P. G., and Obinger, C. (2005) Kinetics of interconversion of ferrous enzyme, compound II and compound III of wild-type *Synechocystis* catalase-peroxidase and Y249F. Proposal for the catalatic mechanism, *J. Biol. Chem*. (in press).
42. Dunford, H. B. (1999) *Heme Peroxidases*, Wiley-VCH, New York.
43. Regelsberger, G., Jakopitsch, C., Engleder, M., Ruker, F., Peschek, G. A., and Obinger, C. (1999) Spectral and kinetic studies of the oxidation of monosubstituted phenols and anilines by recombinant *Synechocystis* catalase-peroxidase compound I, *Biochemistry 38*, 10480−10488.
44. Engleder, M., Regelsberger, G., Jakopitsch, C., Furtmuller, P. G., Ruker, F., Peschek, G. A., and Obinger, C. (2000) Nucleotide sequence analysis, overexpression in *Escherichia coli* and kinetic characterization of *Anacystis nidulans* catalase-peroxidase, *Biochimie 82*, 211−219.
45. Nam, W., Choi, H. J., Han, H. J., Cho, S. H., Lee, H. J., and Han, S.-Y. (1999) Use of 2-methyl-1-phenylpropan-2-yl hydroperoxide (MPPH) as a mechanistic probel for the heterolytic versus homolytic O−O bond cleavage of tert-alkyl hydroperoxide by iron (III) porphyrin complex, *Chem. Commun*., 387−388.
46. Zhao, X., Girotto, S., Yu, S., and Magliozzo, R. S. (2004) Evidence for radical formation at Tyr-353 in *Mycobacterium tuberculosis* catalase-peroxidase (KatG), *J. Biol. Chem. 279*, 7606−7612.
47. Yu, S., Chouchane, S., and Magliozzo, R. S. (2002) Characterization of the W321F mutant of *Mycobacterium tuberculosis* catalase-peroxidase KatG, *Protein Sci. 11*, 58−64.
48. Ivancich, A., Jakopitsch, C., Auer, M., Un, S., and Obinger, C. (2003) Protein-based radicals in the catalase-peroxidase of *Synechocystis* PCC6803: A multifrequency EPR investigation of wild-type and variants on the environment of the heme active site, *J. Am. Chem. Soc. 125*, 14093−14102.
49. Bhaskar, B., Immoos, C. E., Shimizu, H., Sulc, F., Farmer, P. J., and Poulos, T. L. (2003) A novel heme and peroxide-dependent tryptophan-tyrosine cross-link in a mutant of cytochrome *c* peroxidase, *J. Mol. Biol. 328*, 157−166.
50. Gray, H. B., and Winkler, J. R. (1996) Electron transfer in proteins, *Annu. Rev. Biochem. 65*, 537−561.
51. Gray, H. B., and Winkler, J. R. (2003) Electron tunneling through proteins, *Q. Rev. Biophys. 36*, 341−372.
52. Coulson, A. F. W., Erman, J. E., and Yonetani, T. (1971) Studies on cytochrome *c* peroxidase. XVII. Stoichiometry and mechanism of the reaction of compound ES with donors, *J. Biol. Chem. 246*, 917−924.
53. Ho, P. S., Hoffman, B. M., Solomon, N., Kang, C. H., and Margoliash, E. (1984) Kinetics and energetics of intramolecular electron transfer in yeast cytochrome *c* peroxidase, *Biochemistry 23*, 4122−4128.
54. Chouchane, S., Girotto, S., Yu, S., and Magliozzo, R. S. (2002) Identification and characterization of tyrosyl radical formation in *Mycobacterium tuberculosis* catalase-peroxidase (KatG), *J. Biol. Chem. 277*, 42633−42638.
55. Santoni, E., Jakopitsch, C., Obinger, C., and Smulevich, G. (2004) Comparison between catalase-peroxidase and cytochrome *c* peroxidase. The role of the hydrogen-bond networks for protein stability and catalysis, *Biochemistry 43*, 5792−5802.
56. Lukat-Rodgers, G. S., Wengenack, N. L., Rusnak, F., and Rodgers, K. R. (2001) Carbon Monoxide Adducts of KatG and KatG-(S315T) as Probes of the Heme Site and Isoniazid Binding, *Biochemistry 40*, 7149−7157.

BI051463Q